2018

Characteristics of the velocity profile at tidal-stream energy sites

M. Lewis

S. P. Neill

P. Robins

Mohammad Reza Hashemi

S. Ward

Renewable Energy 114 (2017) 258–272

Contents lists available at ScienceDirect

Renewable Energy

journal homepage: www.elsevier.com/locate/renene

Characteristics of the velocity profile at tidal-stream energy sites

M. Lewis [a, c, *], S.P. Neill [a], P. Robins [a, c], M.R. Hashemi [b], S. Ward [a, c]

[a] School of Ocean Sciences, Bangor University, UK
[b] Department of Ocean Engineering and Graduate School of Oceanography, Rhode Island University, USA
[c] Centre of Applied Marine Sciences, Bangor University, UK

ARTICLE INFO

Article history:
Received 21 July 2016
Received in revised form
27 March 2017
Accepted 30 March 2017
Available online 4 April 2017

Keywords:
Tidal energy
Velocity profile
Tidal turbine
ADCP
Irish Sea

ABSTRACT

Realistic oceanographic conditions are essential to consider in the design of resilient tidal-stream energy devices that can make meaningful contributions to global emissions targets. Depth-averaged or simplified velocity profiles are often used in studies of device performance, or device interaction with the environment. We improve representation of flow at tidal-stream energy regions by characterising the velocity profile. At two potential tidal-stream energy sites, the 1/7th power-law with a bed-roughness coefficient of 0.4 accurately described the observed velocity profile on average (>1 month ADCP deployments). Temporal variability in the power-law fit was found at both sites, and best characterised with Generalised Extreme Value distribution; with correlation of variability to tidal condition, wind speed and wave conditions found. The mean velocity profile was accurately simulated using a 3D hydrodynamic model (ROMS) of the Irish Sea (UK) but with temporal variability in accuracy of power-law fits. For all potential tidal sites, the spatial-mean velocity profile was also found to be similar (characterised with ~1/7th power-law and 0.4 bed-roughness value). Therefore realistic flow conditions can be characterised for tidal-energy research, but dynamically coupled wind-wave-tide models, or long-term observations, are needed to fully characterise velocity profile temporal variability.

1. Introduction

The generation of low-carbon electricity is of global importance as a strategy to mitigate the impacts of climate change and to ensure energy security in the coming century. Tidal-stream energy, the conversion of the kinetic energy that resides in tidal currents into electricity (typically through intercepting the flow via arrays of horizontal axis turbines [3]), is favoured as a renewable energy resource for a number of reasons such the predictability of tidal energy to provide firm renewable electricity (e.g. Refs. [15,21,25,48]). For example, the UK government has set a target of 15% renewable energy generation by 2020 [12], with marine energy projected to contribute 4 GW from Welsh waters by 2025 and 27 GW from UK waters by 2050 (www.gov.uk/government/collections/uk-renewable-energy-roadmap). Yet, a lack of knowledge about the range of oceanographic conditions expected at potential tidal stream sites has been identified as a limiting factor to the growth of the industry (e.g., [15,26]). Hence, to meet renewable energy targets and provide the UK with a high-tech globally exportable industry (e.g., [6]); realistic oceanographic conditions at potential tidal-stream energy sites need to be characterised so that resilient, and efficient, tidal-stream energy convertor devices can be designed – reducing the risks and costs of device development (see www.gov.uk/government/collections/uk-renewable-energy-roadmap).

To be economically feasible, tidal-stream energy devices are being positioned in energetic tidal flows, with first generation sites having peak spring tidal current speeds exceeding 2.5 m/s and in water depths between 25 m and 50 m [15]. Hence, tidal-stream energy devices, and their support structures, will be located in the region of flow that experiences friction from the seabed – often called the boundary layer [3]. Friction from the seabed results in reducing tidal velocity (U_z) near to the seabed (i.e. as z reduces), typically referred to as the velocity profile by oceanographers and characterised using the power law of [34] as described in Eq. (1);

$$U_z = \left(\frac{z}{\beta\ h}\right)^{1/\alpha}\ \overline{U} \tag{1}$$

the velocity profile (the velocity at height z above the seabed U_z) is described using a power law (α) and bed roughness (β) coefficient

* Corresponding author.
E-mail address: m.j.lewis@bangor.ac.uk (M. Lewis).

http://dx.doi.org/10.1016/j.renene.2017.03.096

with water depth (h) and depth averaged velocity ($\overline{U}$).

$$U_z = \frac{u_*}{\kappa}\ln\left(\frac{z}{z_0}\right) \quad (2)$$

It should also be noted that the log-law (see Eq. (2) from Ref. [34]) can also be used to characterised the velocity profile (U_z, the velocity at height z above the seabed) using estimates of friction velocity (u_*) and bed roughness length-scale (z_0) with von Karman's constant ($\kappa = 0.4$). However, the power law of Eq. (1), which is derived from shelf-sea oceanographic research (e.g. Refs. [35,36]), is typically used to characterise the velocity profile in tidal energy research (e.g. Refs. [3,21,28]). For example, depth-averaged shallow water-equation models are often used for resource assessment because of their computational efficiency [29], with an assumed velocity profile using the 1/7th power law with a bed roughness (β) of 0.32 within Eq. (1) (e.g. Refs. [3,32]). With the development of high-performance computing systems, resource assessment with high resolution 3D oceanographic models is becoming feasible (e.g. Refs. [30,31,37,38,44]). Yet, it is unclear as to the importance of using a more complex modelling approach; moreover, oceanographic boundary conditions are required for fine-scale modelling studies of turbine interaction with the resource (e.g. Ref. [28]). Hence, methods are required in tidal energy research to estimate the velocity profile (U_z) from depth-averaged flow speed ($\overline{U}$), and therefore the suitability of characterising the velocity profile with the power law profile (Eq. (1)) will be evaluated in this study.

Within the power law velocity profile equation (Eq. (1)), an assumed bed roughness (β) value of 0.32, typically used in shelf-sea oceanographic research (e.g. Refs. [35,36]), may be incorrect at tidal energy sites because seabed sediment is likely to be much coarser, or bed forms that give higher bed roughness values (β), in areas of fast tidal currents [39]. Hence, bias may be present when characterising the velocity profile in tidal energy research because a higher β needed in Eq. (1). Further, although [21] found no significant difference in tidal turbine performance for velocity profiles varying within the range $\alpha = 7$ and $\alpha = 8$ (i.e. 1/7th or 1/8th power law), recent observations at tidal-stream energy sites [26] and EPRI guidelines (see Refs. [7,9]), suggest a 1/10th power law ($\alpha = 10$) should be used when characterising the velocity profile at high tidal energy sites.

Tidal turbine studies typically use scaled tank experiments or device-scale hydrodynamic numerical models (e.g. Refs. [1,21]), with parameterised oceanographic conditions (e.g. Ref. [42]). Variability in the velocity profile has been shown to result in variability to the loadings upon the support structure of a tidal turbine and gearbox [1]; [20], as well as the performance of the tidal energy device [2]. The amount of shear, and hence the velocity profile shape, affects blade loadings, and needs to be considered in fatigue studies [3] because the cyclic loading from the blade rotating through the velocity profile leads to fatigue, and ultimately failure – hence why increasing shear and been shown to increase fatigue of tidal-stream energy but also wake recovery for array design (see Ref. [21]). Therefore, uncertainty of the velocity profile shape at tidal-stream energy sites may be a barrier to research into resilient, efficient, and globally deployable device development.

Surface waves can have a considerable influence on the mean velocity profile in coastal waters [8,17]. An increase in mean upper water-column velocities (increasing velocity shear) occurs under the presence of waves opposing the direction of flow, and the converse occurs when waves propagate in the same direction as the tidal flow (e.g., [14]; [13]; [43]). Therefore, characterising the velocity profile and the amount of velocity shear is essential (e.g. [2,3,7]), if resilient, diversely deployable and efficient, tidal-stream energy convertor devices are to be developed for the global market (see Ref. [27]).

To illustrate the uncertainty within the velocity profile, a range of power law (α) and bed roughness (β) coefficients used within Eq. (1) for tidal-energy research are shown in Fig. 1 in a typical 1st generation site; depth-averaged flow speed ($\overline{U}$) of 2.5 m/s in 40 m water depth (h). The maximum potential turbine swept area (see Refs. [16,17]) is shown as the grey shaded area of Fig. 1, which is assumed to be 5 m above the bed and 5 m below Lowest Astronomical Tide (LAT); assumed in this proof-of-concept example as 35 m, and so LAT is 40 m. The variability in the shape of the velocity profile shown in Fig. 1 is likely to result in variability to predicted turbine device loadings and cyclic loadings from the rotation of the blade through the grey shaded region (e.g. Refs. [20,21]). Furthermore, using Equation (3) (see Refs. [7,9]),

$$P = \sum_{z=5}^{z=LAT-5}\left[\frac{1}{2}\rho A_z \ \delta z\,(u_z)^3\right] \quad (3)$$

where the velocity (u_z) and the swept turbine width at height above the bed z (A_z, with discretised height, δz, being 0.1 m in this case) are used to estimate the theoretical instantaneous power (P), we find the tidal-energy resource varies by +8% (by decreasing α from 7 to 5) to −4% (by increasing α from 7 to 9, with changing β from 0.32 to 0.4 decreasing the power by 9%) for the various velocity profiles in Fig. 1.

Despite the importance of velocity profile characterisation for the effective progression of the tidal-stream energy industry, no

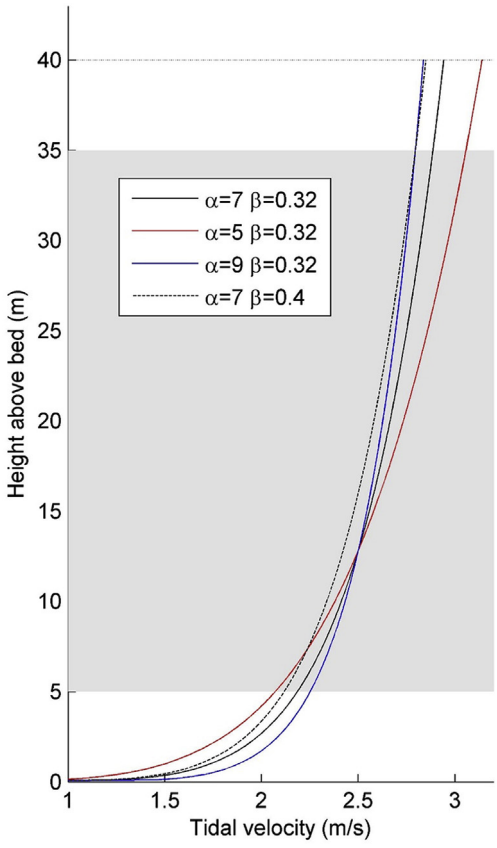

Fig. 1. Velocity profile variability due to uncertainty the power law (α) and bed roughness (β) coefficients of Equation (1) for assumed conditions present at a typical tidal-stream energy site, with the assumed maximum potential turbine swept area shown in grey.

comprehensive investigation has yet been undertaken at strong tidal flow sites [21]. In this paper, we analyse flow data from two field surveys within the highly-energetic Irish Sea, combined with 3D model simulations (see Section 2), which together are used to investigate the spatial and temporal variability of the velocity profile at all potential tidal-stream energy sites; therefore, our results (Section 3) will lead to an improved understanding for the design of a high performance, resilient and globally deployable tidal-stream energy convertors.

2. Methodology

Data from Acoustic Doppler current profiler (ADCP) observations collected at two potential tidal stream energy locations (Section 2.1) were used to calculate vertical velocity profiles characteristics. Temporal deviations in profile characteristics were compared to the corresponding wave climate, which was simulated with a validated SWAN wave model (Section 2.4). Finally, the tidal velocity profile characteristics were analysed for all potential tidal stream energy locations resolved with a well validated 3D tidal model of the Irish Sea (Section 2.4).

2.1. ADCP observations

Data from two ADCPs deployed at potential tidal stream energy sites in the Irish Sea, UK (see Fig. 2), was made available through the SEACAMS project (www.seacams.ac.uk). One ADCP was installed in 33.5 m water depth at Site A (53.4425°N and 4.2976°W), offshore of the port of Amlwch, for ~47.5 days between 10-Feb 2014 and 30-Mar 2014. A second ADCP deployment for 28.6 days between 14-Aug 2013 and 12-Sep 2013 in 86.6 m water depth at Site B (53.3223°N and 4.7883°W), known locally as 'Holyhead Deep'; see Fig. 2. Both instruments were Teledyne 600 kHz ADCPs; with data from both ADCP locations averaged to give hourly velocity profiles that can be compared to other met ocean variables (e.g. simulated wave height; see Section 2.3).

2.2. Power law profile fitting

At each hourly time step in the data-series, when the depth averaged tidal velocity exceeded 1 m/s (likely turbine cut-in velocity; see Ref. [29]), the tidal velocity profile form of Eq. (1) [35,36] was calculated; hence the variability of velocity shear (α variability) and bed roughness (β variability) can be analysed.

To calculate the tidal velocity profile form of Eq. (1), both the power law coefficient (α) and the bed roughness coefficient (β) were iterated through a wide range of values (α varied between 1 and 15, β varied between 0.1 and 1.0) and the most accurate solution recorded, with the accuracy of the velocity profile fit evaluated using the Absolute Error Squared (AES);

$$AES = \int_{z=5}^{z=LAT-5} (Uo_z - Up_z)^2 . \delta z \quad (4)$$

AES is calculated in Equation (4) as the sum of the squared difference of the ADCP observed velocity speed at height z (Uo_z) and that described with every iteration of Eq. (1) (i.e. the predicted current speed at height z; Up_z); with z being each discretised height above the bed (z = 1 m here) between the potential maximum swept area of the turbine. The potential maximum swept area is

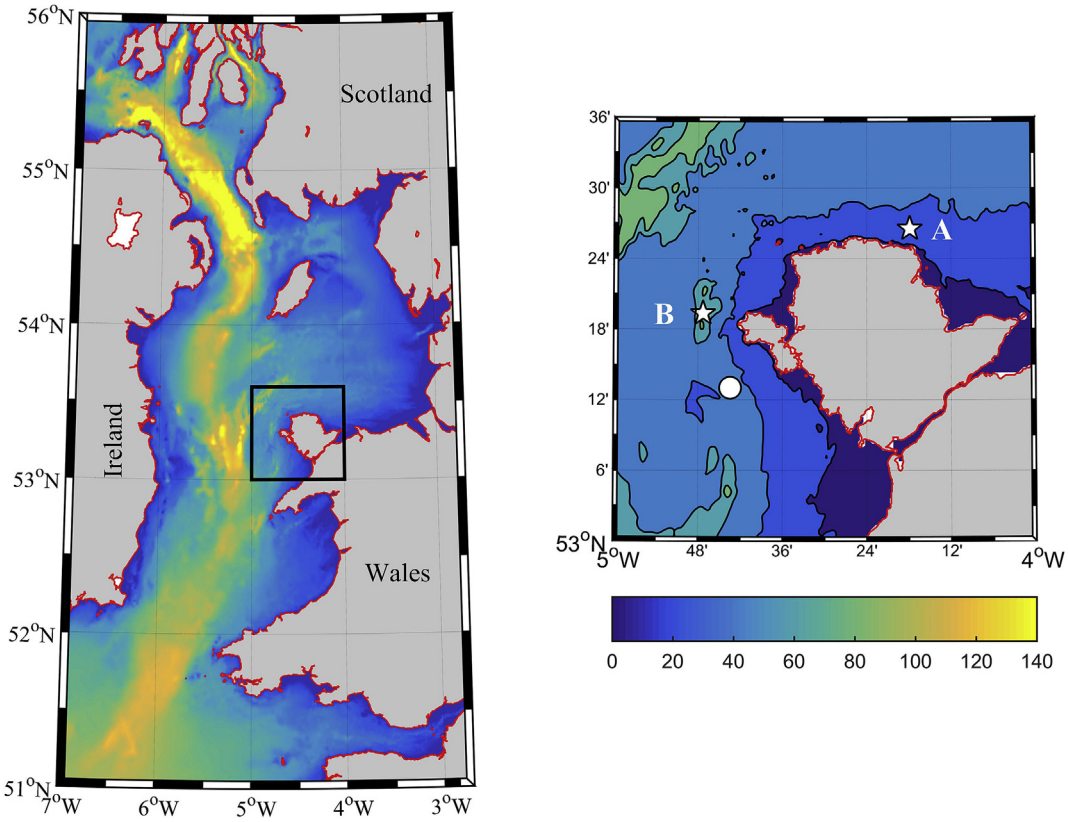

Fig. 2. Bathymetry of the Irish Sea (m rel. to Mean Sea Level), with the location of the two ADCP sites (site A and site B) and the wave buoy (white circle) shown in the enlarged area (right hand figure) of Anglesey. The extent of (a) also corresponds to the subsequent model domain (Sections 2.3 and 2.4).

assumed to be 5 m above the seabed and 5 m below the Lowest Astronomical Tide level [16,17].

The AES described in Eq. (4) was used as a measure of accuracy in the velocity profile fit in this study because the performance of the velocity profile fit for the maximum potential swept area was sort instead of comparing the accuracy between sites (where water depth should be accounted for e.g. using Root Mean Squared Error). Hence the combination of α and β which gives a minimum AES (Eq. (4)) is assumed to give a mathematical description of the tidal velocity profile at each site and time-step.

2.3. Irish Sea tidal model

xTo extrapolate the observed velocity profile characteristics to all potential tidal stream energy sites in the Irish Sea, a 3-Dimensional Regional Ocean Modelling System (ROMS), which simulates tidal hydrodynamics using finite-difference approximations of the Reynolds-Averaged Navier-Stokes (RANS) equations using hydrostatic and Boussinesq assumptions [10,33]. The, ROMS modelling approach has been successfully applied in a number of tidal-stream energy resource studies (e.g. [23,24]). Furthermore, this ROMS model has previously been successfully applied to Irish Sea tidal-stream resource analysis and is well validated; further details of this tidal model can be found in Ref. [15]; and so the model is described only briefly in this paper.

Digitised Admiralty bathymetric data was corrected for mean sea-level variations and were interpolated to the orthogonal (C-grid) computational ROMS domain grid 1/240° fixed longitudinal resolution (see Refs. [15,16]), with ten vertical layers in the Sigma coordinate system (evenly distributed throughout the water column). The Irish Sea model domain and bathymetry are shown in Fig. 2. No wetting and drying scheme was used (minimum depth 10 m), as the geographic scale of inter-tidal regions was relatively small in relation to the model resolution and extent of the Irish Sea [18].

The turbulence closure Generic Length Scale (GLS) model was tuned to the κ-ε turbulence model, as similar results were found across a number of case studies and GLS schemes [40], and good agreement was found for simulated velocity profiles [15]. The open boundary of the tidal model was forced with FES2012 (Finite Element Solution and data assimilated global tide product [5,19]); using ten tidal constituents (M2, S2, N2, K2, K1, O1, P1, Q1, Mf, and Mm). A quadratic bottom drag coefficient (C_D) of 0.005 with a bed roughness size (Z_{ob}) of 0.1 m was chosen after initial comparison to the ADCP data at the two sites (see Ref. [16]).

Tidal model validation was achieved using the same data and methods presented in Ref. [15]: 7 tide gauges from the National Tidal and Sea Level Facility (see www.ntslf.org) and principle semi-diurnal lunar constituent (M2) tidal ellipse comparison at 9 depth-averaged locations (from Ref. [47]), and 131 depth-specific locations from the British Oceanographic Data Centre (www.bodc.ac.uk). The M2 tidal ellipse is described using CMAX (the semi-major ellipse velocity component), CMIN (the semi-minor ellipse velocity component), INC (the inclination of the current ellipse in °N), and phase (degrees relative to Greenwich).

Validation is summarised in Table 1, and includes comparison to the two ADCP sites (A and B) which are described in Section 2.1. Tidal constituents were calculated from hourly output of the simulated elevation and velocities with t_tide [46] for the 30 day simulation; hence the first two days of the simulation were removed to allow the model to spin up from a stationary initial state, and, as shown in Table 1, the Irish Sea model validated extremely well for both elevations and tidal currents (see Ref. [15]).

Table 1
Irish Sea tidal model validation of the principle semi-diurnal lunar constituent (M2), presented as Root Mean Squared Error (RMSE), with normalised RMSE given as a percentage in brackets, for: 7 tide gauges (M2 and principle semi-diurnal solar constituent, S2), 131 tidal current observations at specific depths (east-west (u) and north-south (v) components), 9 sites of depth-averaged M2 tidal ellipse information and the two ADCP locations described in Section 2.2.

Elevation (N = 7)	M2 amplitude	0.12 m (5%)
	M2 phase	28°
	S2 amplitude	0.14 m (16%)
	S2 phase	41°
Depth-averaged currents (N = 9)	CMAX (m/s)	0.06 (8%)
	CMIN (m/s)	0.02 (8%)
	INC	6°
	Phase	8°
tidal currents at specific depths (N = 131)	U amplitude	0.11 m/s (10%)
	U phase	12°
	V amplitude	0.08 m/s (8%)
	V phase	8°
M2 tidal ellipse site A	CMAX	0.06 m/s (5%)
	CMIN (m/s)	0.00 m/s (0%)
	INC	3°
	Phase	6°
M2 tidal ellipse site B	CMAX	0.07 m/s (5%)
	CMIN	0.00 m/s (0%)
	INC	3°
	Phase	6°

2.4. Wave climate simulation

To determine the influence of waves upon the tidal velocity profile, a SWAN [4] wave model was setup for the Irish Sea domain shown in Fig. 1, at a resolution of 1/120° longitude, with variable (1/191° to 1/215°) latitudinal resolution. The model was nested within a coarser outer model of the North Atlantic [22], and both model domains were forced with 3-hourly ERA-Interim wind-fields, at a resolution of 0.75 × 0.75°. The model was validated over the 2 month (July–August 2014) period of a wave buoy deployment ~12 km south of Site B (at 53.217°N, 4.724°W), as shown in Fig. 2, and led to the validation statistics shown in Table 2. Hence, the model has sufficient skill and accuracy to correlate changes in the vertical tidal profile characteristics to the simulated wave climate at ADCP locations A and B.

3. Results

The ADCP velocity profile observations at two potential tidal-stream energy sites (Section 2.1) are presented in Section 3.1, with temporal variability in the velocity shear quantified and compared with the simulated wave climate and wind climate. The spatial variability of velocity profile characteristics, extrapolated to all potential tidal-stream energy sites in a shelf sea environment (Section 2.3), is presented in Section 3.2.

3.1. Observations

Tidal ellipse analysis of tidal velocity data from ADCP deployments at the two potential tidal-stream energy sites is shown

Table 2
Wave model validation statistics for significant wave height (*Hs*) and energy wave period (*Te*) for July–August 2014. RHO is the Pearson correlation coefficient, S.I. is the scatter index (RMSE normalised by the mean of the observations), and bias is the mean of the simulated values minus the mean of the observations.

Variable	RHO	RMSE	S.I.	bias
Hs	0.96	0.09 m	0.067	−0.15 m
Te	0.67	1.40 s	0.264	0.09 s

Table 3
Depth-averaged tidal ellipse information for the two major tidal constituents (M2 and S2), calculated from ADCP data at two potential tidal-stream energy sites.

Site	location	Deployment length (days)	water depth (m)	Const.	Frequency (3 d.p)	CMAX (m/s)	CMIN (m/s)	INC (°N)	Phase (° rel. GMT)
A	53.44°N 4.30°W	47.5	33.5	M2	0.081	1.22	0.02	166	38
				S2	0.083	0.49	0.01	166	84
B	53.33°N 4.79°W	28.6	86.6	M2	0.081	1.31	0.11	76	229
				S2	0.083	0.48	0.04	75	273

Table 4
Average velocity profile fitting parameters (Eq. (1)) from ADCP observations at the two potential tidal-stream energy sites (A and B). Errors within each velocity profile fit (using Eq. (2)) are summed.

		Site A	Site B
Power law fit (α)	range (min & max)	4–14	4–15
	mean	7.1	7.1
	standard deviation	1.2	2.2
bed roughness fit (β)	range (min & max)	0.30–0.50	0.30–0.50
	mean	0.40	0.41
	standard deviation	0.03	0.03
Sum of absolute error (AES) of fit		0.0054	0.1374

in Table 3 for both the principle semi-diurnal lunar (M2) and solar (S2) constituents, which together describe the spring-neap tidal cycle. The rectilinear nature of the tidal currents can be seen by the ratios of CMAX (the semi-major ellipse velocity component) and CMIN (the semi-minor ellipse velocity component) in Table 3. The Lowest Astronomical Tide (LAT) is calculated as 3.6 m (site A) and 2.4 m (site B) below Mean Sea-Level based on the simulated tidal elevation amplitudes of the 6 major constituents; M2, S2, K1, O1, N2 and K2 [15]. Hence, the maximum swept area of the turbine is assumed to extend between 5 m above the seabed to 29.9 m (above the seabed) at site A and 79.2 m (above the seabed) at site B. Velocities were measured with the ADCP from 2.6 m to 4.7 m above the seabed at sites A and B respectively, with the top 3 "bins" removed from both ADCP data series (3 m for site A and 6 m for sites B) due to surface effects; therefore, ADCP data can be used to evaluate the velocity profile within the maximum swept area.

The coefficients of the velocity profile characterisation are summarised in Table 4 for both ADCP sites. Examples of the most and least accurate velocity profile fits are shown in Fig. 3 for site A and Fig. 4 for site B. The low sum of the absolute error squared (AES) in the velocity profile fitting (see Section 2.2) gives confidence in the accurate description of the hourly averaged vertical structure of tidal velocity (see Table 4), and is demonstrated in Figs. 3 and 4; therefore the velocity profile were successfully characterised using Eq. (1) for all depth-average flow speeds above 1 m/s (the likely cut-in speed of a tidal turbine [29] shown as a green line in Figs. 4 and 5); see Table 4. The larger sum of AES at Site B, in Table 4, is likely due to the greater water depth relative to Site A (see Table 3).

When averaged throughout the ADCP deployment, the velocity profile parameters (α and β) were similar for both sites to one significant figure; see Table 4. Therefore, it could be assumed that the 1/7th power law with a bed roughness value of 0.4 within Eq. (1) is appropriate to use when characterising the velocity profile of

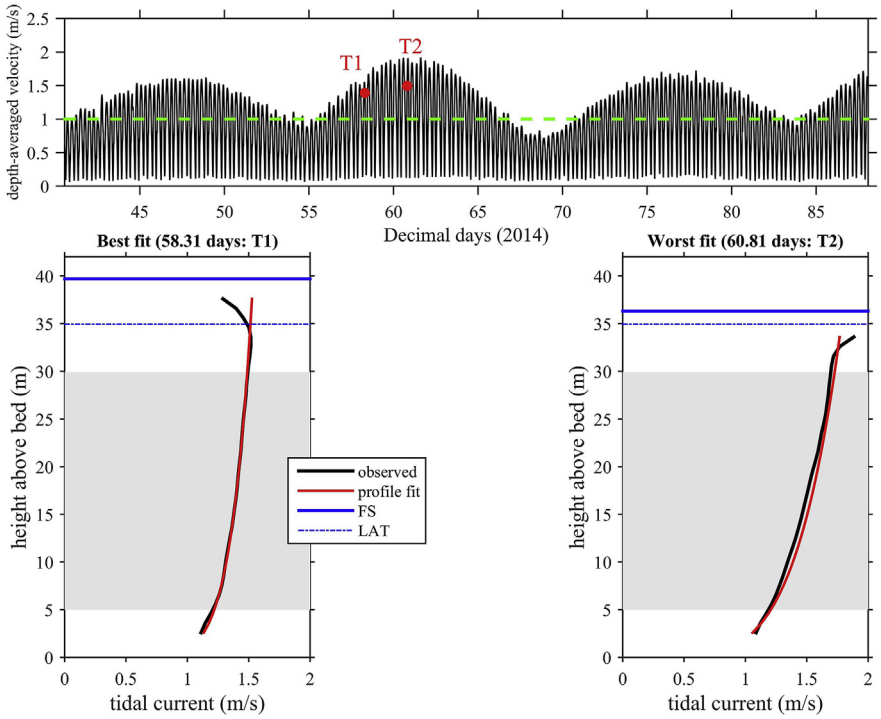

Fig. 3. The depth-averaged velocity time-series (top panel) measured at site A. Two examples (T1 and T2) of the velocity profile fit are shown in the bottom panels: Best fit (T1) with an AES of 0.00 m^2/s on the left hand bottom panel, and the least-accurate profile fit (T2) with an AES of 0.03 m^2/s on the right hand bottom panel. The free surface (FS) is shown in the velocity profiles (bottom panels), and grey shaded area indicating the maximum potential swept tidal turbine area, assumed as 5 m above the bed and 5 m below the Lowest Astronomical Tide (LAT).

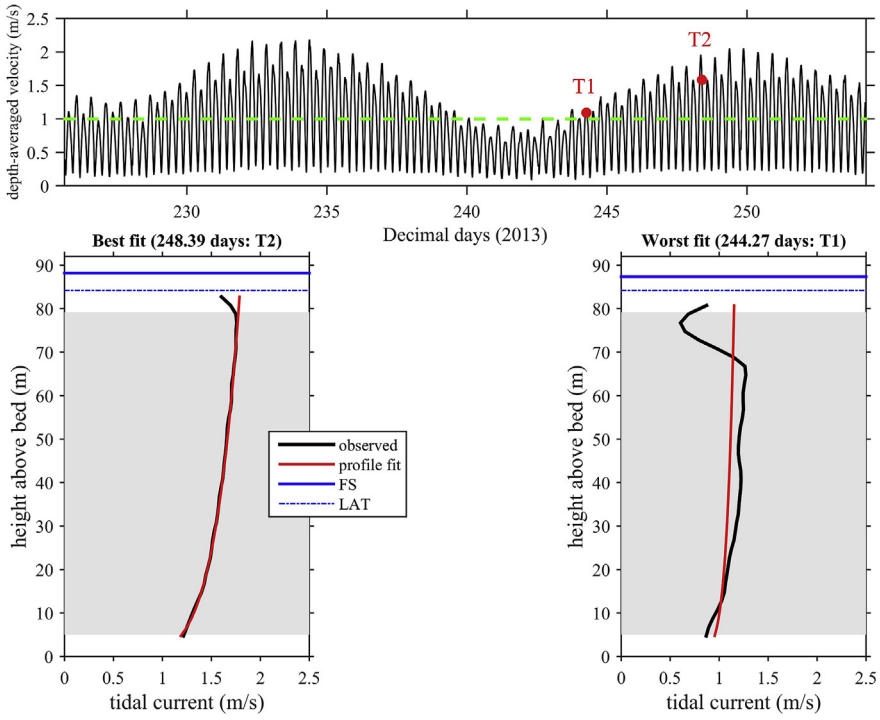

Fig. 4. The depth-averaged velocity time-series (top panel) and velocity profile fit examples for the site B; the least-accurate profile fit (T1) with an AES of 2.35 m^2/s, and the best profile fit (T2) with an AES of 0.00 m^2/s. Potential swept area is shown as grey shaded area in bottom panels and the green line in the top panel shows 1 m/s, above which velocity profile fits are analysed. (For interpretation of the references to colour in this figure legend, the reader is referred to the web version of this article.)

a tidal energy site from depth-averaged tidal current information. However, temporal variability with the power law (α) was found at both ADCP sites; with α standard deviation (S.D.) of ~1 at site A and ~2 at site B, and a range of α fits from 4 to 15, whilst little β fit temporal variability was observed (see Table 4).

Velocity profile coefficient fits (α and β) were grouped into tidal conditions; flooding or ebbing tide, tidal velocity accelerating or decelerating or at "peak" (maximum flow speed in the hourly averaged data). A two sample Kolmogorov-Smirnov test (KStest), with a null hypothesis that the two groups of data are from the same continuous distribution at the 5% significance level, was performed on the velocity profile coefficients α and β (see Table 5). For both ADCP deployments, the KStest revealed β fits were broadly similar at all tidal states, but with a small difference between flooding and ebbing β values at Site B (flooding currents were 0.01 higher, see Table 5). Power law (α) fits were significantly different when grouped into tidal conditions (see Table 5), and can be seen clearly in the probability distributions of α fits in Fig. 5. Further, the distribution of temporal variability of power law (α) fits (Fig. 5), was found to be most accurately described by a generalised extreme value (GEV) distribution (rather than a normal distribution using the KStest) at both sites; see Appendix Figs. A1 and A2.

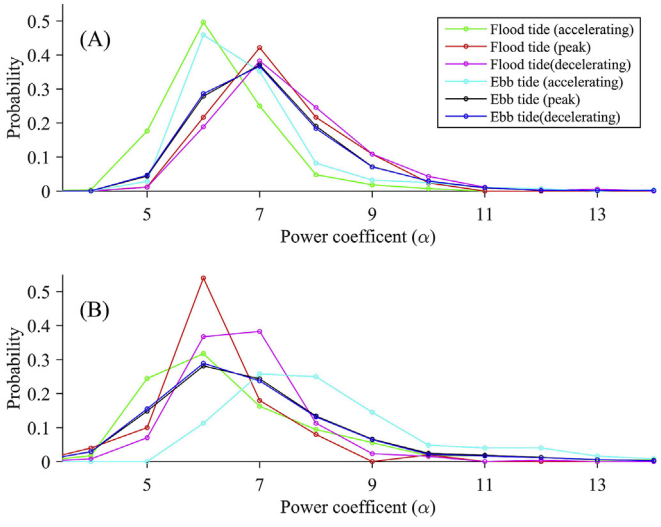

Fig. 5. The distribution of the power coefficient (α) of observed velocity profile fits when grouped into statistically similar tidal regimes (e.g. flooding) for (A) site A and (B) site B.

The grouped velocity profile coefficient fits (α and β) of Table 5 (and shown in Fig. 5 for α) were correlated to depth-averaged current speed ($\overline{U}$) using Pearson Correlation (RHO values at the 5% significance level) and linear regression (R^2). No significant correlation of β fits to depth-averaged current speed was found at either site A or B (see Table 5; all R^2 values were 0% and RHO values below 0.01 at both sites). Conversely, correlations of α fits to depth-averaged flow speed ($\overline{U}$) were significant (at the 5% significance level) for all tidal conditions at site A, with the amount of velocity shear increasing (lower α fits) as flow speed increased (negative RHO values in Table 5) and all flooding tidal conditions (accelerating, peak or decelerating) exhibiting the same trend of high velocity shear (low α fits) with larger $\overline{U}$ values (but with different degrees of significance, see Table 5), whilst only accelerating ebb current α fits were found to significantly correlate to $\overline{U}$ (but with the opposite trend to flooding tidal conditions). At site B, a significant trend (higher α with increasing $\overline{U}$) was found for all flood tide α fits, with the converse (lower α with increasing $\overline{U}$) found for all ebb tide data (see Table 5).

Table 5
Analysis of the velocity profile fits (α and β) at two potential tidal-stream energy sites (A and B) when depth-averaged flow speeds ($\overline{U}$) are above 1 m/s; grouped into tidal conditions, with the similarity of these grouped distributions evaluated with a KStest (KSstat and pvalue displayed; distributions similar at the 5% significance level are marked in bold) and these statistically similar groups correlated to $\overline{U}$ (using the Pearson correlation, RHO with pvalue in brackets, and linear regression scores, R^2) with significant correlations (at the 5% significance level - based on RHO, sample number (N) and pvalues) marked in bold.

	tidal conditions	N	Mean & (S.D.)		mean AES with fit	Similarity of group (KS stat & pvalue)		Correlation between α fits and $\overline{U}$	
			α	β		α	β	Rho (pvalue)	R^2
Site A	All tidal currents	347	7.1 (1.2)	0.40 (0.03)	0.005	0.16 & 0.00	**0.04 & 0.61**	**−0.28 (0.00)**	**8%**
	All flood tidal currents	150	6.9 (1.3)	0.40 (0.03)	0.007	0.49 & 0.00	–	**−0.41 (0.00)**	**17%**
	All ebb tidal currents	197	7.3 (1.2)	0.40 (0.03)	0.005	0.38 & 0.00	–	−0.09 (0.19)	1%
	Peak ebb tide	73	7.4 (0.9)	0.40 (0.02)	0.004	**0.08 & 0.94**	–	0.00 (0.99)	0%
	Peak flood tide	78	7.3 (1.0)	0.40 (0.02)	0.005			**−0.17 (0.14)**	**3%**
	accelerating ebb tide	45	6.8 (1.2)	0.39 (0.03)	0.006	0.19 & 0.00	–	**0.27 (0.07)**	**7%**
	accelerating flood tide	35	6.3 (0.9)	0.41 (0.03)	0.009			**−0.39 (0.02)**	**15%**
	Decelerating ebb tide	79	7.6 (1.1)	0.40 (0.02)	0.003	0.9 & 0.17	–	0.08 (0.47)	1%
	Decelerating flood tide	37	7.5 (1.3)	0.40 (0.02)	0.005			**−0.35 (0.03)**	**12%**
Site B	All tidal currents	238	7.1 (2.2)	0.41 (0.03)	0.137	0.19 & 0.00	0.13 & 0.00	0.01 (0.89)	0%
	All flood tidal currents	129	6.9 (2.0)	0.41 (0.04)	0.133	0.20 & 0.00)	**0.04 & 1.00**	**0.22 (0.01)**	**5%**
	All ebb tidal currents	109	7.4 (2.4)	0.40 (0.02)	0.143	0.48 & 0.00	**0.06 & 0.92**	**−0.24 (0.01)**	**6%**
	Peak ebb tide	41	7.9 (1.9)	0.40 (0.01)	0.071	0.50 & 0.00)	–	0.15 (0.35)	2%
	Peak flood tide	47	6.6 (2.0)	0.40 (0.02)	0.100			**−0.39 (0.01)**	**15%**
	accelerating ebb tide	19	8.7 (2.5)	0.41 (0.03)	0.092	0.47 & 0.00	–	**−0.47 (0.04)**	**22%**
	accelerating flood tide	44	7.0 (2.5)	0.41 (0.04)	0.218			**0.39 (0.01)**	**15%**
	Decelerating ebb tide	49	6.6 (2.0)	0.40 (0.01)	0.184	0.26 & 0.00	–	**−0.26 (0.07)**	**7%**
	Decelerating flood tide	38	6.9 (1.3)	0.42 (0.04)	0.044			**−0.34 (0.03)**	**12%**

As the temporal variability of the grouped α fits (i.e. spread in the distributions of Fig. 5) cannot be explained by the correlation to current speed alone (see Table 5), hourly velocity profile fits of α and β were next compared to the simulated wave climate and associated wind fields (interpolated from the forcing wind data of the wave model). The results of this correlation are shown in Table 6 for site A, and Table 7 for site B, which had a relatively less energetic wave climate during the deployment period (as can be seen in Fig. 7 compared to Fig. 6). The β fits at the shallower site A (all tidal conditions) significantly correlated to the simulated wave power (and wave period), with lower bed roughness values (β) during larger waves. Significantly higher bed roughness values were also found with higher wave heights and wind speeds at site B, with the exception of ebb tidal conditions – see Tables 6 and 7.

Velocity shear was found to significantly decrease (higher α fits) with larger waves for flood tide conditions (accelerating and decelerating; see Table 7) at site A, and the converse true for decelerating ebb tidal conditions. At site B, significant negative correlation to peak flooding tidal conditions reveals a general increase in the amount of velocity shear with more energetic wave conditions (height, period or power), which was also found in ebb tidal conditions (with the exception of decelerating flows) for greater wind speeds (see Table 7). Furthermore, wind speed was also found to have some significant correlation to the grouped power law fits; however, no clear relationship between the wind speed or wave properties, and the parameters used to characterise the velocity profile (α and β) were found at either site; summarised in Tables 6 and 7, and is demonstrated in Fig. 8.

Finally, analysis of the depth averaged currents revealed a significant correlation to the wave conditions. The daily value of the major axis (CMAX) of the semi diurnal lunar tidal constituent ellipse (M2), calculated from a moving 25 h over-lapping analysis window of ADCP measured depth averaged currents (using t_tide and based on the method of [41], revealed weaker M2 tidal currents with larger daily averaged significant wave heights (Hs); see Fig. 9.

Table 6
The linear regression score (R^2) and Pearson correlation score (RHO and PVAL) for the comparison of velocity profile fitting parameters (α and β) at site A to the simulated wave climate; significant wave height (Hs) and zero-crossing wave period (Tz), and the interpolated wind fields. Significant Pearson Correlations at the 5% level are highlighted in bold.

Profile fitting parameter:		β fits	α fits						
Tidal condition group:		all	peak currents (flood & ebb)	flooding tide			ebbing tide		
				increase	Peak	decrease	increase	Peak	Decrease
Number of fits (N)		347	151	35	78	37	45	73	79
Wave height (*Hs*)	RHO	−0.08	0.01	0.29	0.20	0.42	−0.15	−0.27	−0.23
	PVAL	0.11	0.93	0.09	0.08	0.01	0.32	0.02	0.03
	R^2	1%	0%	9%	4%	18%	2%	7%	6%
Wave period (*Tz*)	RHO	**−0.19**	0.07	**0.40**	**0.23**	**0.35**	**0.22**	−0.13	−0.08
	PVAL	**0**	0.38	**0.02**	**0.04**	**0.04**	**0.15**	0.26	0.46
	R^2	**4%**	1%	**16%**	**4%**	**12%**	**5%**	4%	1%
Wave power	RHO	**−0.09**	−0.03	**0.43**	**0.25**	**0.48**	−0.07	**−0.27**	**−0.21**
	PVAL	**0.09**	0.68	**0.01**	**0.03**	**0.00**	0.65	**0.02**	**0.06**
	R^2	**1%**	0%	**18%**	**6%**	**23%**	0%	**7%**	**5%**
Wind speed	RHO	0.03	−0.04	0.05	0.06	−0.01	**−0.28**	**−0.19**	−0.09
	PVAL	0.57	0.66	0.76	0.58	0.95	**0.06**	**0.11**	0.41
	R^2	0	0%	0%	0%	0%	**8%**	**3%**	1%

Table 7
The linear regression score (R^2) and Pearson correlation score (RHO and PVAL) for the comparison of velocity profile fitting parameters (α and β) at site B to the simulated wave climate; significant wave height (*Hs*) and zero-crossing wave period (*Tz*), and the interpolated wind fields. Significant Pearson Correlations at the 5% level are highlighted in bold.

Profile fitting parameter:		β fits		α fits					
Tidal condition group:		flood (all)	ebb (all)	flooding tide			ebbing tide		
				increase	Peak	decrease	increase	Peak	decrease
Number of fits (N)		130	109	44	47	38	19	41	49
Hs	RHO	0.12	0.12	0.04	−0.20	0.06	0.03	0.06	0.07
	PVAL	0.18	0.22	0.79	0.18	0.73	0.91	0.72	0.64
	R^2	1%	1%	0%	4%	0%	0%	0%	0%
Tz	RHO	0.11	0.10	0.07	**−0.21**	0.04	0.00	0.09	**0.18**
	PVAL	0.23	0.32	0.66	**0.16**	0.79	0.99	0.59	**0.21**
	R^2	1%	1%	0%	**4%**	0%	0%	1%	**3%**
Wave Power	RHO	0.09	0.09	0.03	**−0.20**	0.03	−0.04	0.04	0.08
	PVAL	0.34	0.37	0.84	**0.18**	0.87	0.87	0.78	0.59
	R^2	1%	1%	0%	**4%**	0%	0%	0%	1%
Wind speed	RHO	**0.17**	**0.14**	0.05	**0.06**	−0.01	**−0.28**	**−0.19**	−0.09
	PVAL	**0.05**	**0.16**	0.76	**0.58**	0.95	**0.06**	**0.11**	0.41
	R^2	**3%**	**2%**	0%	0%	0%	**8%**	**3%**	1%

Table 8
Comparison of accuracy between the observed and simulated velocity profile power law fit (α of Eq. (1)) at ADCP sites A and B. Average difference in the hourly power law fit (δα) including standard deviation (s.d. shown in brackets) and Pearson Correlation coefficient at the 5% significance level (RHO) between δα and the simulated wave climate (significant wave height, Hs) for the grouped tidal conditions.

Tide direction	Tidal flow condition	Site A		Site B	
		Mean (s.d.)	RHO	Mean (s.d.)	RHO
Flood	accelerating	−1.2 (0.9)	−0.02	−1.6 (0.9)	0.06
	Peak	−0.6 (1.0)	0.01	−1.3 (0.9)	0.07
	decelerating	−0.6 (1.0)	0.00	−1.2 (0.7)	0.06
Ebb	accelerating	0.0 (0.4)	−0.08	0.3 (1.0)	0.23
	Peak	0.0 (0.0)	0.00	−0.5 (0.7)	0.02
	decelerating	0.7 (0.5)	−0.06	−1.6 (0.9)	0.22
All hourly conditions		−0.7 (0.8)	0.08	−1.1 (1.1)	0.08

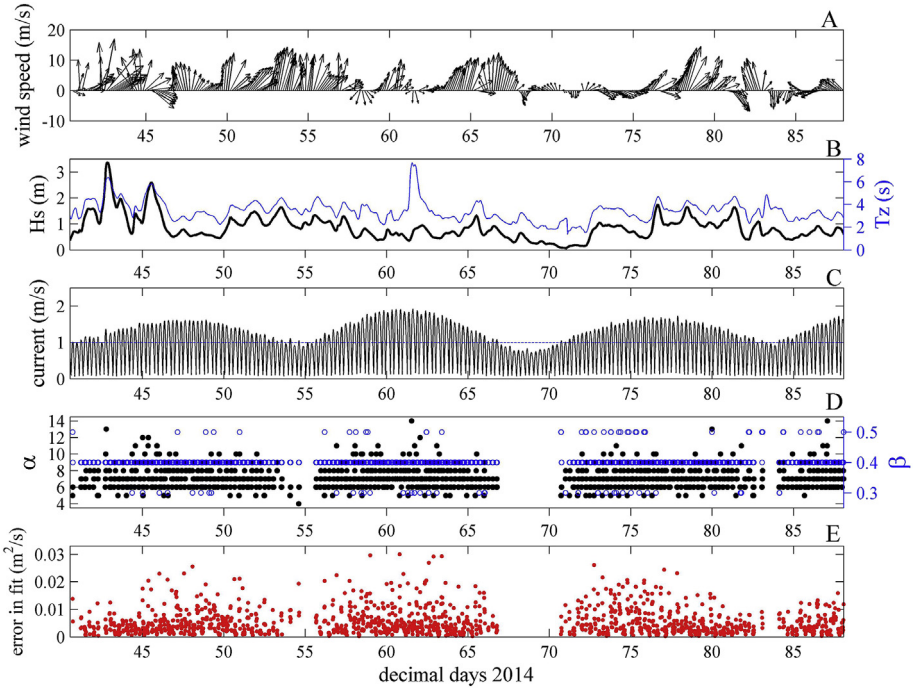

Fig. 6. Simulated wave climate (panel B) and the associated interpolated local wind field data (A) for the ADCP data-series (depth-averaged velocity shown in C with 1 m/s likely cut-in speed shown) observed at site A compared to the velocity profile fit coefficients α and β (D, left and right axes, respectively), and error in the velocity profile curve fit (E).

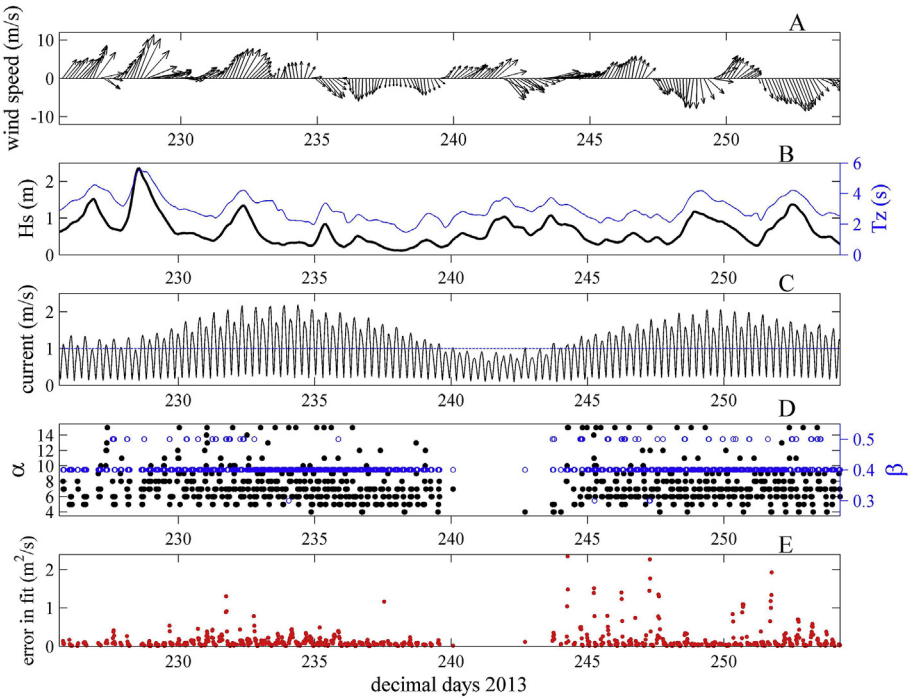

Fig. 7. Simulated wave climate (B) and the associated interpolated local wind field data (A) for the ADCP data-series (C) observed at site B compared to the velocity profile fit coefficients α and β (D, left and right axes, respectively), and error in the velocity profile curve fit (E).

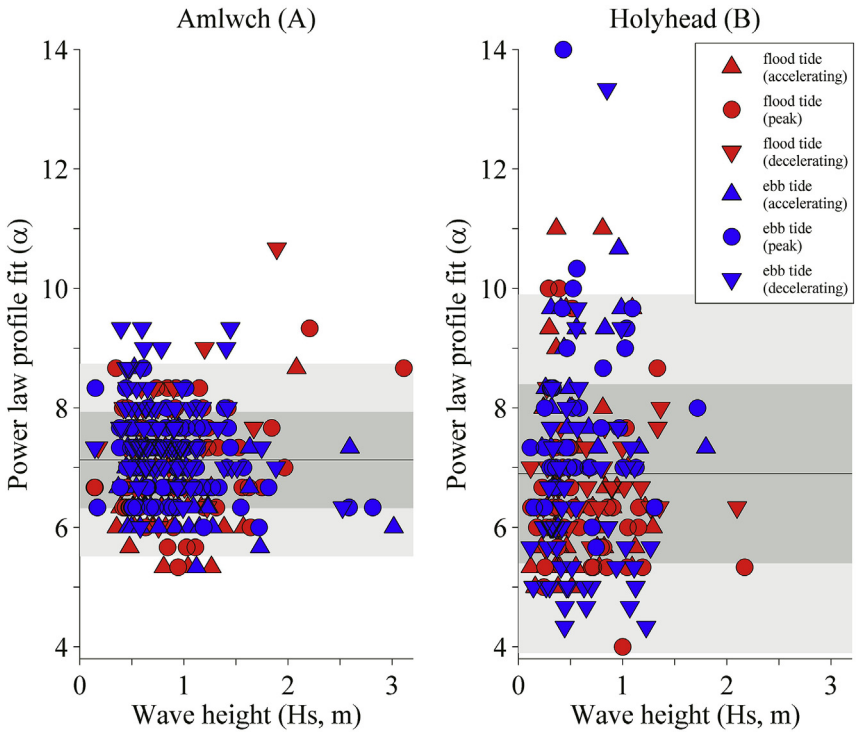

Fig. 8. The comparison between the power law fit (α) of the curve fit to the hourly ensemble average ADCP data and the simulated significant wave height (Hs) at the two potential tidal-stream energy sites: A and B. The average power law fit (α) for all tidal conditions is shown as a black line with 68% (darker shading) and 95% (lighter shading) confidence intervals shown.

Analysis of the trend in Fig. 9 showed a Pearson correlation of −0.21 (4% R^2) and −0.29 (8% R^2) for sites A and B respectively. Therefore, some evidence suggests wind-waves influence the velocity profile at tidal-stream energy sites, both in magnitude (Fig. 9) and shape (Figs. 6 and 7), however, the processes driving this temporal variability appear complex and non-linear.

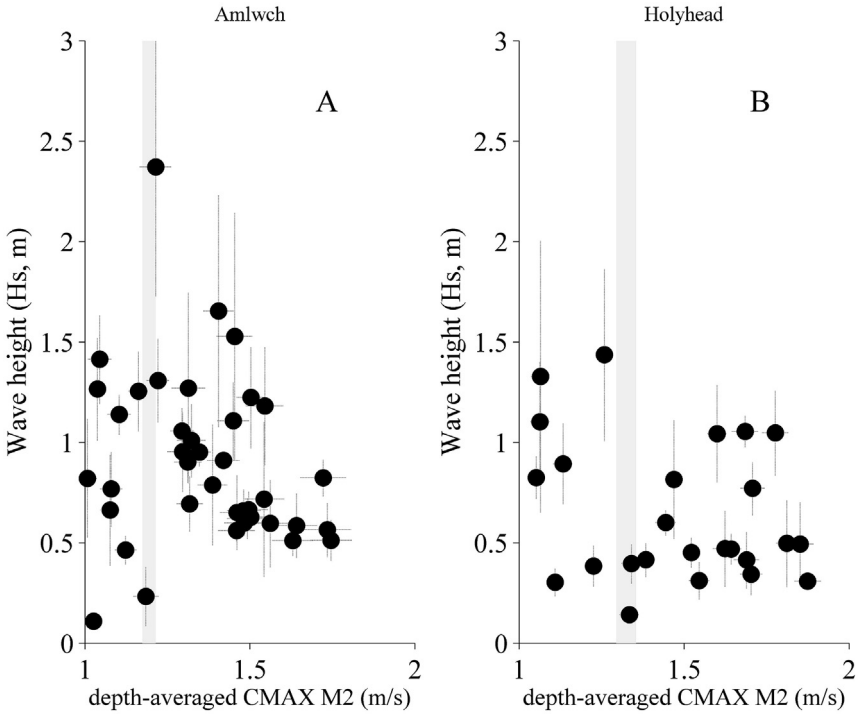

Fig. 9. The depth-averaged semi-major axis of the semi diurnal lunar tidal constituent ellipse (CMAX M2), calculated from a 25 h over-lapping analysis window, of ADCP measured at sites A and B, compared to the average significant wave height simulated during the same time period (the range of simulated daily wave heights are show as dashed lines). The shaded region is the CMAX M2 calculated from the entire ADCP deployments (see Table 3).

3.2. Velocity profile spatial variability

The validated ROMS model of the Irish Sea (see Section 2.3) was applied to simulate tidal current velocities during the period of the two ADCP deployments. The accuracy of ROMS simulated depth average M2 tidal ellipse at the two ADCP sites is shown in Table 1 (<5% error in current speed), and the tidal velocity profile (velocities throughout the water-column) was accurately simulated at both sites with less than 1% velocity errors (RMSE ~0.15 m/s).

Model velocity profile fits (α and β) were compared at both ADCP locations, and a good agreement found on average (see Table 8); bed roughness (β) fits were exactly simulated at both sites (mean β fit difference of 0.0 with 0.0 standard deviation hence not shown in Table 8), and α fit difference of −0.7 (standard deviation of 0.8) at site A and −1.1 (standard deviation 1.1) at site B was calculated (difference calculated between ADCP data fits and model fits). Therefore the ROMS hydrodynamic model simulates the shape of the velocity profile accurately on average, but with temporal variability in accuracy (see Table 8) and a small amount of bias as the over-prediction of shear in the water column by the model as α fits of the model are consistently lower (see Table 8).

Improvements to this temporal variability in the accuracy of the ROMS tide-only α fits from the simulated velocity profile shape (see Table 8) is likely to require a dynamically coupled wave-tide model (e.g. Ref. [15]); however, the tide-only hydrodynamic model can be used to determine the likely spatial variability of the average velocity profile characteristics (α and β) at potential tidal-stream energy sites as the model accurately simulated the velocity profile shape and magnitude on average (see Table 8 and also Table 1).

Analysing the spatial variability of the mean power law fit (α) in the 30 day ROMS Irish Sea hydrodynamic model simulation for all potential tidal-stream energy sites in the Irish Sea was not trivial, requiring ~27 million iterations to determine the average α and β fits at all potential tidal-stream energy sites – assumed to be at sites with a peak spring tidal current (M2+S2) above 1.8 m/s and with water depths 25 m or greater [15,16]. All sites analysed were estimated to have the boundary layer (δ) extend to the surface and hence Eq. (1) can be used. The depth of the boundary layer (δ) was estimated using [36], see Equation (5),

$$\delta = 0.0038\left(\frac{\overline{u}_a\sigma - \overline{u}_b f}{\sigma^2 - f^2}\right) \quad [5]$$

in which we assume an M2 tidal frequency (σ) of $1.4052^{*}10^{-4}$ rad/s, with maximum depth-averaged current speed of the major ($\overline{u}_a$) and minor ($\overline{u}_b$) M2 tidal ellipse information taken from the ROMS model with latitude (φ, to calculate f in Eq. (5); $f = 1.4544{*}10^{-4}\sin(\varphi)$) also taken at each grid cell in the model domain.

The typical spring-neap α and β fits of all theoretical tidal-stream energy sites throughout the Irish Sea are shown in Fig. 10; indicating that whilst β fits were broadly similar, there was some trend in the spatial variability of average velocity profile shape (α), which is of importance to developers for site selection: an average α fit of 6.7 and a β fit of 0.4 was found (standard deviation of 2.2 and 0.1 for α and β fits respectively) and a trend of decreasing shear with increased water depth (R^2 of 57% in panel d of Fig. 10) was found when grouping sites into 20 m water depth bins, but no significant trend was found for peak spring tidal currents (R^2 of 4% in panel c of Fig. 10).

Considering the small amount of bias in the model (resulting in slightly lower α fits by the model), we assumed an average $\alpha = 7$ fit is likely to generally be appropriate for characterising the velocity profile (with $\beta = 0.4$ in Eq. (1)) at shelf sea tidal energy sites, with less shear likely (higher α) at deeper water sites which may be important for the development of future device technologies, such

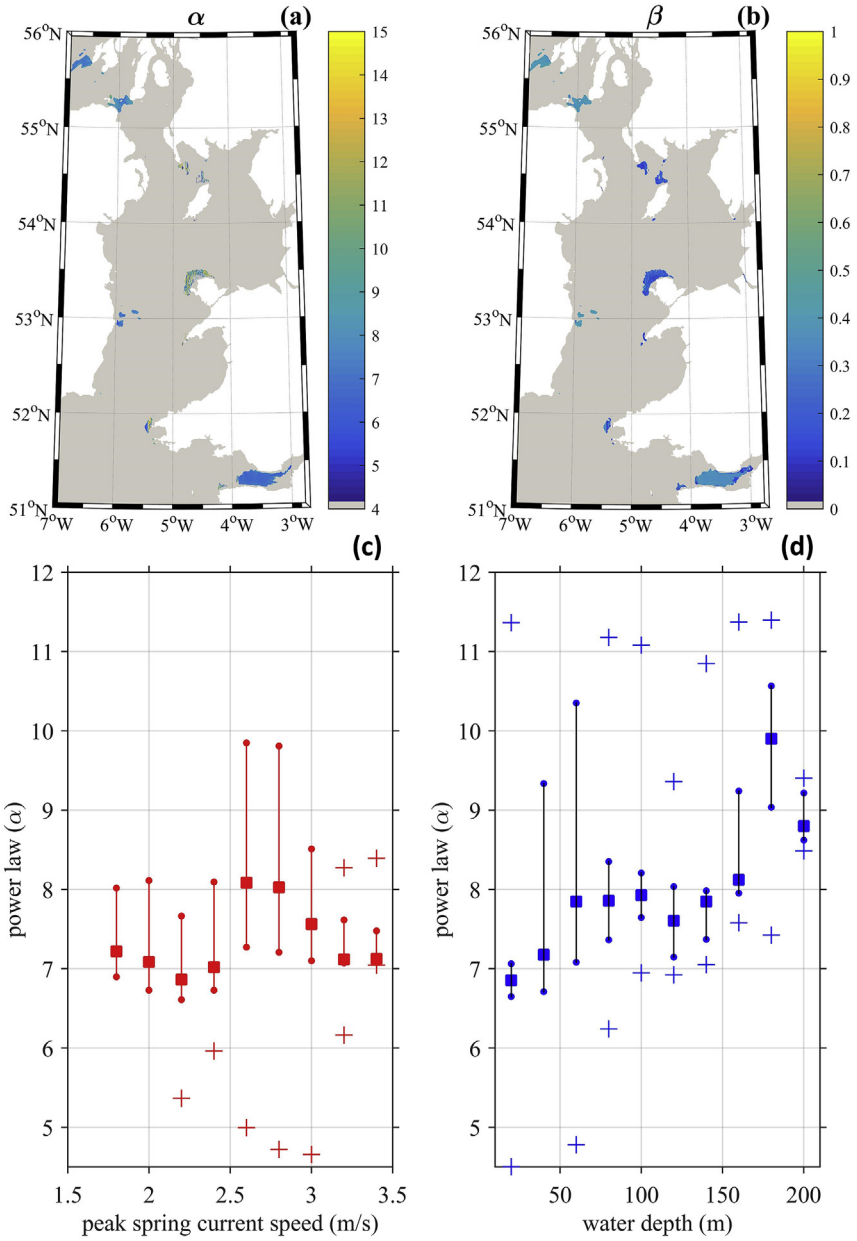

Fig. 10. The mean power law (α fit in panel A) and bed roughness (β fit in panel b) for all potential tidal-stream energy sites simulated for a typical spring-neap cycle with the ROMS hydrodynamic model of the Irish Sea (peak spring tidal velocities above 1.8 m/s and water depths > 25 m), including the mean power law trend (squares), with 25th and 75th quantiles (shown as solid dots) and 1st and 99th quantiles (crosses) when grouped into 0.2 m/s current (panel c) and 20 m depth bins (panel d).

as so-called 2nd generation devices (see Ref. [15]). However, observations (or possibly dynamically coupled wave-tide models) are required to quantify the temporal variability to this average velocity profile characteristics and, we find, GEV (Generalised Extreme Value) theory can be used to describe this temporal variability within α fits.

4. Discussion

The velocity profile was accurately characterised at two tidal energy sites using a classical power law (Eq. (1)). Both sites had similar profile parameters when reported to one decimal place and averaged over the time of the observations. Therefore when characterising the velocity profile of a tidal energy site in depth-averaged model resource studies or turbine interaction studies (e.g. Refs. [3,21]), it appears appropriate to assume a 1/7th power law, within Eq. (1), which is traditionally used by oceanographers (see Ref. [36]). Moreover, a bed roughness value of 0.4, within Eq. (1), was found to yield a more accurate fit (with observations) on average than the value of 0.32 suggested by Ref. [36]. This enhanced bed roughness coefficient, calculated from ADCP velocity profile fits at two potential tidal-stream energy sites, is likely due to coarser sediment types (or larger bed forms) in these tidally-energetic environments (see Ref. [39]), and this enhanced bed roughness ($\beta = 0.4$) should be considered in future studies of turbine interaction with the resource.

Temporal variability in the power law (α) fit at both ADCP sites was observed during likely operating times ($\overline{U} > 1$ m/s), with

times of extremely high shear tidal flow (i.e. $\alpha = 4$), which has important implications for turbine performance and resilience research (e.g. Ref. [1]) as well as the instantaneous power available – as described in the introduction (see also [17]). The distribution of power law (α) temporal variability was accurately characterised with Generalised Extreme Value (GEV) theory; hence, future studies of turbine-scale interaction with the resource (e.g. Ref. [21]) can use such distributions to explore extreme loadings upon the device and the support structure (e.g. Ref. [20]), or improve the parameterised oceanographic conditions within scaled-tank experiments or CFD models (see Refs. [21,42]). We have therefore provided the GEV parameters used to describe the α fit distribution in the Appendix Table A1, which is shown in Appendix Figs. A1 and A2. Indeed, future work could also aim to resolve sub-hourly variability of the velocity profile, such as turbulent fluctuations (e.g. Refs. [1,45]).

Power law (α) temporal variability was found to correlate significantly (at 5% significance level with Pearson correlation) with the tidal condition, which could be due to the influence of local-scale bathymetric features on generating localised turbulence; for example, accelerating flows at site A and the flooding tidal conditions at site B were found to be typically more sheared (lower α fits). Hence, developers should be aware of fine-scale spatial variability in oceanographic conditions that may exist, which suggests detailed site surveys are essential during later stages of resource assessment (e.g. Refs. [7,9]). Furthermore, temporal variability within the power law fits (α) were found to correlate to wind speed, the wave climate, and tidal current speed. For example, with an increase in simulated wave heights generally resulting in more shear (lower α fit) during ebb tidal conditions for the shallower site A, and the converse for site B. Therefore, future work should apply a dynamically coupled model; especially as the presence of waves was found to retard the depth averaged flow, as hypothesised by Refs. [17] and [11].

Temporal variability of the velocity profile was not accurately simulated with the tide-only Irish Sea 3D ROMS model of [15]; which is expected, considering the lack of wave processes included in the model; however, the mean simulated velocity profile shape was found to match extremely well at both ADCP sites. Hence, the ROMS model was used to explore the spatial variability in mean velocity profile characteristics at potential tidal-stream energy sites throughout the Irish Sea (see Fig. 10). Spatial variability to the mean power law coefficient was found in the Irish Sea, suggesting site selection an important process but that spatial variability appears to be less than temporal variability (i.e. Fig. 10 and Table 4); therefore, variability in the velocity profile characteristics at potential tidal-stream energy sites in shelf sea environments (i.e. shallow, well mixed, fast tidal current environments) can be captured and quantified.

A trend of decreasing shear with increasing water depth was found (R^2 57%); therefore, the development of deeper water tidal-stream energy device technologies could result in more resilient devices, as the loadings from shear would be reduced (e.g. Ref. [21]). Simulated averaged spatial variability was found to be much less than the observed temporal variability; hence the challenge remains to fully characterise the structure of flow at tidal-stream energy sites so a widely deployable device could be achieved. We find that future work should develop and apply dynamically coupled 3D models to inform the industry of extreme and mean hydrodynamic conditions to inform the design of a globally deployable and resilient device.

5. Conclusions

The vertical structure of flow at tidal-stream energy sites was characterised using ADCP observations at two sites, and a well validated 3D ROMS tidal model was used to extrapolate characteristics of the simulated velocity profile to all potential tidal-stream energy sites in the Irish Sea – a typical high tidal-energy shelf sea region. The spatial and temporal variability in the velocity profile was found to be an important uncertainty to characterize in tidal-stream energy research, but also has applications to coastal processes and coastal engineering. On average the 1/7th power law ($\alpha = 7$) with roughness coefficient $\beta = 0.4$ was found to accurately represent the velocity profile (based on classical oceanography theory), yet both spatial and temporal variability was found for potential tidal-stream energy sites throughout the Irish Sea.

Temporal variability of the power law was found to be large at both ADCP sites and could be described by Generalised Extreme Value theory distribution. Wave and hydrodynamic (i.e. tidal) conditions did not independently account for observed temporal variability in the power law fits that describe the velocity profile; suggesting, where observations are unavailable or impractical, dynamically coupled wind-wave-tide models are required to fully characterise oceanographic conditions at tidal-stream energy sites. Further, although temporal variability of the roughness coefficient was found to be almost negligible, the inclusion of the roughness coefficient was found to be essential to accurately describe the velocity profile. Finally, simulated spatial variability of the vertical structure of the flow (i.e. between potential shelf sea tidal-stream energy sites) appears to be much less than observed temporal variability; hence, a widely, possibly even globally, deployable device design is possible, reducing barriers to development within the tidal-stream energy industry and allowing meaningful contributions to global low carbon energy targets.

Acknowledgments

SPN and MJL wish to acknowledge the support the Sêr Cymru National Research Network for Low Carbon, Energy and the Environment (NRN-LCEE) and the EPSRC Supergen project EP/J010200/1. PR and SW acknowledges the support of the SEACAMS project, which is part-funded by the European Union's Convergence European Regional Development Fund, administered by the Welsh Government (Grant number: 80284). ADCP data was kindly provided by SEACAMS and quality controlled by MJL. The authors also wish to thank two anonymous reviewers whose comments on an earlier draft of this manuscript helped improved the final accepted version.

Appendix

The comparison of Generalised Extreme Value (GEV) and a normal distribution for the grouped velocity power law fits (α) for all tidal velocity profiles when the depth-average flow speed was greater than 1 m/s at site A (Fig. A1) and site B (Fig. A2). The parameters used to describe the GEV distributions of each of the grouped α fit distributions, including the KStest result that shows the GEV distribution to be a more accurate description of these distributions than a normal distribution, is shown in Table A1 for both ADCP sites.

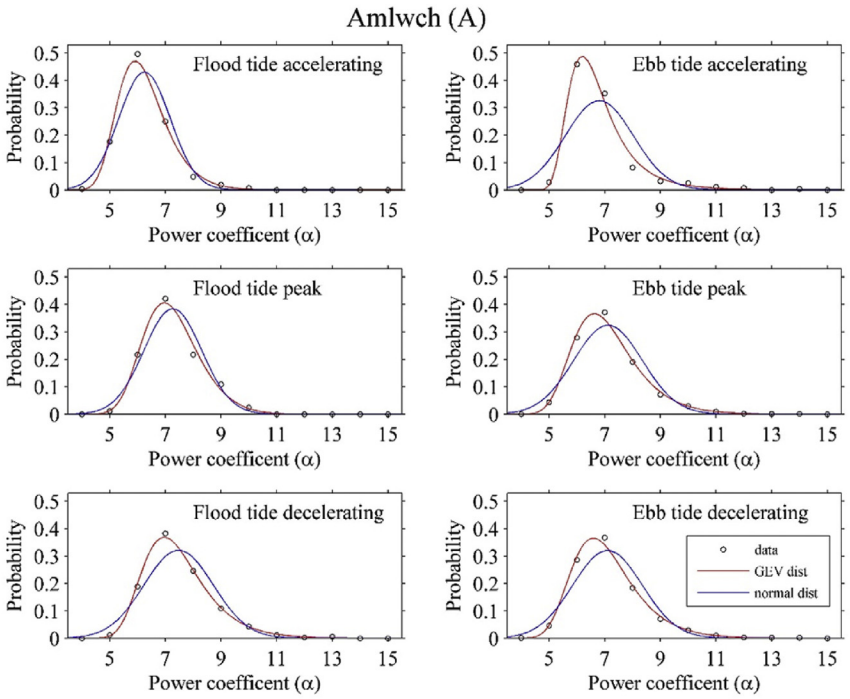

Fig. A1. Comparison of Generalised Extreme Value (GEV) distribution and normal distribution for the grouped velocity power law fits of the ADCP record at site A (Amlwch) for all tidal velocities above 1 m/s.

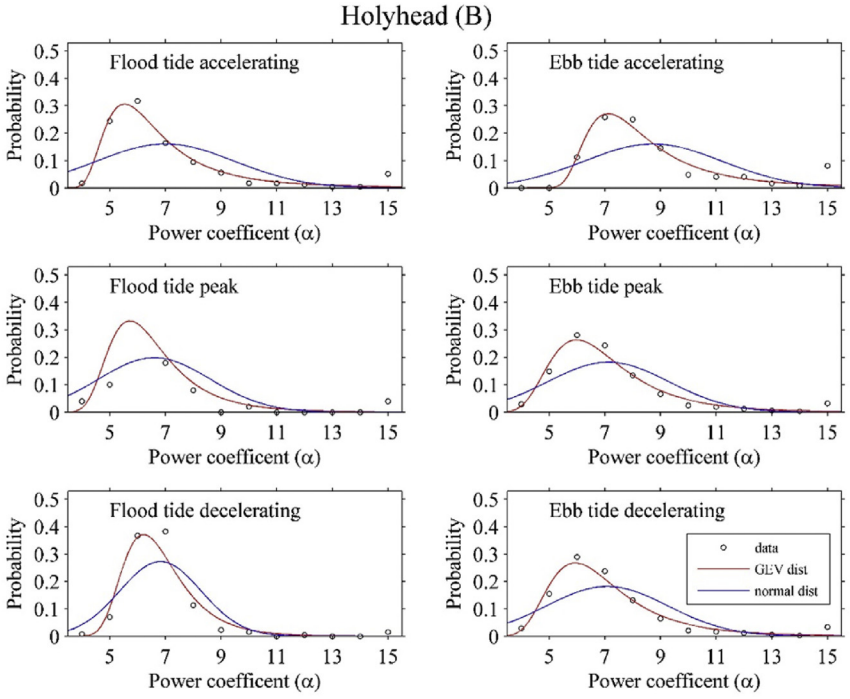

Fig. A2. Comparison of Generalised Extreme Value (GEV) distribution and normal distribution for the grouped velocity power law fits of the ADCP record at site B (Holyhead) for all tidal velocities above 1 m/s.

Table A1
The Generalised Extreme Value (GEV) fit parameters used to describe the temporal variability of the tidal condition grouped power law fits (α) at two ADCP sites (A and B), and the results of the KStest (Kstat & pvalue, with significant correlations at the 5% level given in bold) that show the GEV distribution is a more accurate description of the α distribution than a normal distribution.

		GEV distribution fit parameters			KS test (Kstat & pvalue)	
		Shape	Scale	Location	Normal distribution	GEV distribution
Site A	Flood accelerating	−0.0689	0.7828	5.8496	0.37 & >0.01	0.53 & 0.02
	Flood peak	−0.1243	0.9133	6.8349	0.37 & >0.01	**0.40 & 0.14**
	Flood decelerating	−0.0279	0.9977	6.9272	0.35 & >0.01	**0.40 & 0.14**
	Ebb accelerating	0.1086	0.7579	6.2737	0.40 & >0.01	**0.40 & 0.14**
	Ebb peak	−0.0404	1.0051	6.5835	0.31 & >0.01	**0.27 & 0.59**
	ebb decelerating	−0.0339	1.0069	6.5598	0.30 & >0.01	**0.27 & 0.59**
Site B	Flood accelerating	0.2775	1.2449	5.8207	0.29 & <0.01	**0.20 & 0.89**
	Flood peak	0.0998	1.1097	5.8255	0.32 & <0.01	0.53 & 0.02
	Flood decelerating	0.0275	0.9901	6.2384	0.36 & <0.01	**0.40 & 0.14**
	Ebb accelerating	0.2788	1.4066	7.4559	0.25 & 0.01	**0.27 & 0.59**
	Ebb peak	0.1137	1.4041	6.1361	0.31 & <0.01	**0.20 & 0.89**
	ebb decelerating	0.1219	1.3836	6.0938	0.30 & <0.01	**0.20 & 0.89**

References

[1] I. Afgan, J. McNaughton, S. Rolfo, D. Apsley, T. Stallard, P. Stansby, Turbulent flow and loading on a tidal stream turbine by LES and RANS, Int. J. Heat. Fluid Flow. 43 (2013) 96–108.

[2] A.S. Bahaj, A.F. Molland, J.R. Chaplin, W.M.J. Batten, Power and thrust measurements of marine current turbines under various hydrodynamic flow conditions in a cavitation tunnel and a towing tank, Renew. Energy 32 (3) (2007) 407–426.

[3] W.M.J. Batten, A.S. Bahaj, A.F. Molland, J.R. Chaplin, The prediction of the hydrodynamic performance of marine current turbines, Renew. Energy 33 (5) (2008) 1085–1096.

[4] N. Booij, R.C. Ris, L.H. Holthuijsen, A third-generation wave model for coastal regions: 1. Model description and validation, J. Geophys. Res. Oceans 104 (C4) (1999) 7649–7666.

[5] L. Carrère, F. Lyard, M. Cancet, A. Guillot, L. Roblou, FES2012: a new global tidal model taking advantage of nearly 20 years of altimetry, in: Proceedings of Meeting 20 Years of Altimetry, Venice, 2012.

[6] R.H. Charlier, A "sleeper" awakes: tidal current power, Renew. Sustain. Energy Rev. 7 (6) (2003) 515–529.

[7] S. Gooch, J. Thomson, B. Polagye, D. Meggitt, Site characterization for tidal power, in: OCEANS 2009, MTS/IEEE Biloxi-Marine Technology for Our Future: Global and Local Challenges, IEEE, 2009, October, pp. 1–10.

[8] J. Groeneweg, G. Klopman, Changes of the mean velocity profiles in the combined wave–current motion described in a GLM formulation, J. Fluid Mech. 370 (1998) 271–296.

[9] G. Hagerman, B. Polagye, R. Bedard, M. Previsic, Methodology for Estimating Tidal Current Energy Resources and Power Production by Tidal In-stream Energy Conversion (TISEC) Devices, EPRI North American Tidal In Stream Power Feasibility Demonstration Project, 2006.

[10] D.B. Haidvogel, H. Arango, W.P. Budgell, B.D. Cornuelle, E. Curchitser, E. Di Lorenzo, et al., Ocean forecasting in terrain-following coordinates: formulation and skill assessment of the regional ocean modeling system, J. Comput. Phys. 227 (7) (2008) 3595–3624.

[11] M.R. Hashemi, S.P. Neill, P.E. Robins, A.G. Davies, M.J. Lewis, Effect of waves on the tidal energy resource at a planned tidal stream array, Renew. Energy 75 (2015) 626–639.

[12] A.S. Iyer, S.J. Couch, G.P. Harrison, A.R. Wallace, Variability and phasing of tidal current energy around the United Kingdom, Renew. Energy 51 (2013) 343–357.

[13] P.H. Kemp, R.R. Simons, The interaction between waves and a turbulent current: waves propagating against the current, J. Fluid Mech. 130 (1983) 73–89.

[14] P.H. Kemp, R.R. Simons, The interaction between waves and a turbulent current: waves propagating with the current, J. Fluid Mech. 116 (1982) 227–250.

[15] M. Lewis, S.P. Neill, P.E. Robins, M.R. Hashemi, Resource assessment for future generations of tidal-stream energy arrays, Energy 83 (2015a) 403–415.

[16] M. Lewis, S.P. Neill, P.E. Robins, S. Ward, M. Piano, M.R. Hashemi, Observations of flow characteristics at potential tidal-stream energy sites, in: European Wave and Tidal Energy Conference 2015, Nantes, France, 2015.

[17] M.J. Lewis, S.P. Neill, M.R. Hashemi, M. Reza, Realistic wave conditions and their influence on quantifying the tidal stream energy resource, Appl. Energy 136 (2014a) 495–508.

[18] M.J. Lewis, S.P. Neill, A.J. Elliott, Interannual variability of two offshore sand banks in a region of extreme tidal range, J. Coast. Res. 31 (2) (2014b) 265–275.

[19] F. Lyard, F. Lefevre, T. Letellier, Francis. O. Modelling the global ocean tides: modern insights from FES2004, Ocean Dyn. 56 (5–6) (2006) 394–415.

[20] A. Mason-Jones, D.M. O'Doherty, C.E. Morris, T. O'Doherty, Influence of a velocity profile & support structure on tidal stream turbine performance, Renew. Energy 52 (2013) 23–30.

[21] L.E. Myers, A.S. Bahaj, Experimental analysis of the flow field around horizontal axis tidal turbines by use of scale mesh disk rotor simulators, Ocean Eng. 37 (2) (2010) 218–227.

[22] S.P. Neill, M.R. Hashemi, Wave power variability over the northwest European shelf seas, Appl. Energy 106 (2013) 31–46.

[23] S.P. Neill, M.R. Hashemi, M.J. Lewis, Optimal phasing of the European tidal-stream resource using the greedy algorithm with penalty function, Energy 73 (2014b) 997–1006.

[24] S.P. Neill, M.R. Hashemi, M.J. Lewis, The role of tidal asymmetry in characterizing the tidal energy resource of Orkney, Renew. Energy 68 (2014a) 337–350.

[25] S.P. Neill, M.R. Hashemi, M.J. Lewis, Tidal energy leasing and tidal phasing, Renew. Energy 85 (2016) 580–587.

[26] F. O'Rourke, F. Boyle, A. Reynolds, Ireland's tidal energy resource; an assessment of a site in the Bulls Mouth and the Shannon Estuary using measured data, Energy Convers. Manag. 87 (2014) 726–734.

[27] F.O. O'Rourke, F. Boyle, A. Reynolds, Marine current energy devices: current status and possible future applications in Ireland, Renew. Sustain. Energy Rev. 14 (3) (2010) 1026–1036.

[28] T. O'Doherty, A. Mason-Jones, D.M. O'Doherty, P.S. Evans, C.F. Wooldridge, I.A. Fryett, Considerations of a horizontal axis tidal turbine, Proc. ICE-Energy 163 (3) (2010) 119–130.

[29] P.E. Robins, S.P. Neill, M.J. Lewis, Impact of tidal-stream arrays in relation to the natural variability of sedimentary processes, Renew. Energy 72 (2014) 311–321.

[30] P.E. Robins, S. Neill, M. Lewis, S. Ward, Characterising the spatial and temporal variability of the tidal-stream energy resource over the northwest European shelf seas, Appl. Energy 147 (2015) 510–522.

[31] T. Roc, D.C. Conley, D. Greaves, Methodology for tidal turbine representation in ocean circulation model, Renew. Energy 51 (2013) 448–464.

[32] S. Serhadlıoğlu, T.A. Adcock, G.T. Houlsby, S. Draper, A.G. Borthwick, Tidal stream energy resource assessment of the Anglesey Skerries, Int. J. Mar. Energy 3 (2013) e98–e111.

[33] A.F. Shchepetkin, J.C. McWilliams, Regional ocean model system: a split-explicit ocean model with a free-surface and topography-following vertical coordinate, Ocean Model. 9 (2005) 347–404.

[34] R. Soulsby, Dynamics of Marine Sands: a Manual for Practical Applications, Thomas Telford, 1997.

[35] R.L. Soulsby, J.D. Humphery, Field observations of wave-current interaction at the sea bed, in: Water Wave Kinematics, Springer Netherlands, 1990, pp. 413–428.

[36] R.L. Soulsby, L. Hamm, G. Klopman, D. Myrhaug, R.R. Simons, G.P. Thomas, Wave-current interaction within and outside the bottom boundary layer, Coast. Eng. 21 (1–3) (1993) 41–69.

[37] J. Van Der Molen, P. Ruardij, N. Greenwood, Potential environmental impact of tidal energy extraction in the Pentland Firth at large spatial scales: results of a biogeochemical model, Biogeosciences 13 (2016) 2593–2609.

[38] T. Wang, Z. Yang, A. Copping, A modeling study of the potential water quality impacts from in-stream tidal energy extraction, Estuaries Coasts 38 (1) (2015) 173–186.

[39] S.L. Ward, S.P. Neill, K.J. Van Landeghem, J.D. Scourse, Classifying seabed sediment type using simulated tidal-induced bed shear stress, Mar. Geol. 367 (2015) 94–104.

[40] J.C. Warner, C.R. Sherwood, H.G. Arango, R.P. Signell, Performance of four turbulence closure methods implemented using a generic length scale method, Ocean Model. 8 (2005) 81–113.

[41] J. Wolf, D. Prandle, Some observations of wave–current interaction, Coast. Eng. 37 (3) (1999) 471–485.

[42] P.A. Work, K.A. Haas, Z. Defne, T. Gay, Tidal stream energy site assessment via three-dimensional model and measurements, Appl. Energy 102 (2013)

510–519.
[43] S.Q. Yang, S.K. Tan, S.Y. Lim, S.F. Zhang, Velocity distribution in combined wave–current flows, Adv. Water Resour. 29 (8) (2006) 1196–1208.
[44] Z. Yang, T. Wang, A. Copping, S. Geerlofs, Modeling of in-stream tidal energy development and its potential effects in Tacoma Narrows, Washington, USA. Ocean Coast. Manag. 99 (2014) 52–62.
[45] M. Togneri, M. Lewis, S. Neill, I. Masters, Comparison of ADCP observations and 3D model simulations of turbulence at a tidal energy site, Renew. Energy. 114 (Part A) (2017) 273–282, http://dx.doi.org/10.1016/j.renene.2017.03.061.
[46] R. Pawlowicz, B. Beardsley, S. Lentz, Classical tidal harmonic analysis including error estimates in MATLAB using T_TIDE, Comput. Geosci. 28 (2002) 929–937.
[47] J.E. Jones, Charts of the 01, k1, n2, m2 and s2 tides in the celtic sea including m2 and s2 tidal currents, Inst. Oceanogr. Sci. (1983) 59. Report No. 169.
[48] M.J. Lewis, A. Angeloudis, P.E. Robins, P.S. Evans, S.P. Neill, Influence of storm surge on tidal range energy, Energy 122 (2017) 25–36.